J Ther Eng, Vol. 10, No. 2, pp. 457−478, March, 2024

Journal of Thermal Engineering
Web page info: https://jten.yildiz.edu.tr
DOI: 10.18186/thermal.1456700

Journal of Thermal Engineering

Research Article

Principal parameters of thermoelectric generator module design for effective industrial waste heat recovery

Wan Ahmad Najmi Wan MOHAMED[1], Nur Faranini ZAMRI[1], Muhammad Fairuz REMELI[1,*]

[1]*School of Mechanical Engineering, College of Engineering, University Teknologi MARA (UiTM), Shah Alam, 40450, Malaysia*

ARTICLE INFO

Article history
Received: 19 May 2022
Accepted: 25 January 2023

Keywords:
CHP; Energy Recovery; Heat Sink; Thermoelectric Generator; Waste Heat

ABSTRACT

In the sustainable energy agenda, thermoelectric generators (TEG) can be a central technology for low-cost combined heat and power (CHP) systems. TEG module (TEM) is the combination of TEG cells, heat pipes, heat sinks and copper blocks that produce electrical power and thermal energy for low temperature heating simultaneously. Two TEG cells were used in each TEM for CHP in a bakery factory with a reference waste heat temperature of 250°C. Different designs of TEM affect the heat transfer mechanics through the components. However, actual testing of each design requires high cost and time consuming. Identifying the principal parameters affecting the desired output is indeed important before investing in actual design fabrication. One-dimensional model is developed in this manuscript to evaluate the fundamental interactions between each component. Parametric variation for nine main parameters characterized the steady-state response of each parameter under four novel heat sink configurations. The parameter sweeps approach benefits in designing a novel TEM for optimum system output. An improved TEM with 6 TEG cells was designed and it increased the heat recovery ratio from an initial 14% to 38%. The Reynolds number of streams are the major operating parameter as it influences the heat sink effectiveness. Large heat exchanger frontal area and copper block housing surface area are also significant parameters. Identification of these principle parameters would assist in effective designs of TEM systems for industrial CHP.

Cite this article as: Mohamed WANW, Zamri NF, Remeli MF. Principal parameters of thermoelectric generator module design for effective industrial waste heat recovery. J Ther Eng 2024;10(2):457−478.

INTRODUCTION

The development of efficient, low-cost and passive technologies for waste heat recovery (WHR) systems is required for energy sustainability. Harvesting waste heat could generate outcomes that can be reused and supplied back to processes that operate at a lower temperature [1]. Efforts to utilize industrial waste heat are still in progress due to temperature and cost limitations for the use of advanced waste heat recovery cycles [2]. Hybrid technologies for simultaneous heat utilization and electrical generation from waste heat, or Combined Heat and Power (CHP), are mostly ready

***Corresponding author.**
*E-mail address: fairuz1299@uitm.edu.my

This paper was recommended for publication in revised form by Regional Editor Zerrin Sert

and proven at lab-scale but not commercially available. Direct thermal-to-electrical energy conversion can be realized using a thermoelectric generator (TEG) that directly generates electrical power when TEG is positioned between a heat source and a heat sink in a phenomenon called the Seebeck effect [3,4]. TEG is a solid-state semiconductor that excites free electrons, small in size, and requires no maintenance [5,6]. Although the current efficiency of the TEG is less than 5% [7], NASA Jet Propulsion Laboratory revealed obtaining 20% TEG conversion efficiency [8] while new TEG materials and superlattice configurations have increased the figure-of-merit (ZT) up to 2.4 [9]. These advances indicate that electrical generation from industrial waste heat is economically practical in the future.

TEG cell is capable of producing electrical power for a wide range of practical applications. Higher temperature gradient across the junctions generate higher electromotive force and electrical output [10]. Maneewan and Chindaruksa [11] installed a TEG system on a biomass dryer and obtained 1W of power output with a thermal efficiency of 4%. Kaibe et al. [12] tested 16 TEG cells in a carburizing furnace and generated 240W of electrical power with a temperature difference of 220°C. The heat from a blast furnace produced 0.93 kW/m2 TEG power density or equivalent to 2% efficiency [13]. A study by Orr et al. [14] developed a design with 8 TEG cells and produced 54W of electricity from automotive exhaust. TEGs are also used in supporting advanced energy systems including fuel cells [15] and regenerative ORC systems [16] to improve energy utilization efficiency. In automotive application, a 30-cells TEG module was produced by Mohamed [17] which generated 392W power output while a two-stage TEG system was developed for vehicle exhaust by Liu et al. [18] and produced 250W of electricity. Nader [19] conducted a simulation analysis on different TEG setups for hybrid electric vehicles showed a potential for better fuel economy. Chen et al. [20] combined heat collector, TEG and water-cooled heat sinks to improve the efficiency of the waste heat recovery system while Alegria et al. [21] applied different heat exchangers configuration for lower thermal resistance and optimum efficiency of the thermoelectric modules.

The main issue that holds back TEG utilization in practical application is the low conversion efficiency of the technology. Researchers are not only focusing on improving the TEG itself, but also developing and testing different combinations of TEG and other technologies for system optimization. Weng et al. [22] numerically introduced an angle function method of the PN legs inside the TEG and the system performance improved by 35% with 30% higher thermal stress. Chen et al. [23] developed a mathematical model to determine the effect of converging angle in a heat exchanger on the output performance of a TEG system and the performance improved by 12.5%. Alahmer et al. [24] compared different types of cooling mode and Zheng et al. [25] applied passive evaporative cooling heat sink to improve the heat transfer across the TEG technology. For photovoltaic TEG system, Badr et al. [26] analyzed the TEG system efficiency by comparing different passive cooling methods with the highest system efficiency improvement of 28.45%.

TEG technology has been explored mainly for medium-temperature thermal systems for simultaneous electrical and thermal energy generation. Utilizing a stove and finned heat exchanger, Mahdi et al. [27] generated 12.2W from 3 TEG cells to charge a 12V battery as well as transfer 235W for circulating water heating. Montecucco et al. [28] proposed a TEG system for CHP generation from a stove that raised the circulating water temperature by 20^{0}C with an average thermal power of 582W transferred through the TEG. Research by Zhang et al. [29] integrated high-temperature nanostructured TEG cells into a residential gas-fired condensing boiler to create micro combined heat and power systems. An economizer with 4 TEG cells by Zarifi et al. [30] generated 44W of electricity and 1785W of thermal energy. CHP for low-grade waste heat was explored by Zhou et al. [31] using 30 TEG cells for domestic water heating leading to a total of 85.1% system efficiency. A numerical study by Liu et al. [32] developed a TEG system model, validated with experimental data before comparing the effect of three heat sinks on the output performance of a TEG system.

A thermoelectric module (TEM) is a configuration where the TEG is integrated with heat exchangers where it absorbs heat from a hot waste stream, allows the heat to flow effectively across the TEG cells, and then dissipates the heat to a cooler fluid stream that needs heating for CHP generation. TEM is usually built with three sub-sections – two sections of heat sinks connected via heat pipes to a section housing the TEG cells. Heat pipes have high thermal conductivities in the range of 2100–50000 W/m.K [33]. It minimizes heat loss significantly which is an important factor in the logistics of WHR system designs [34]. A heat sink is a device for effective convection heat transfer with a fluid medium. The combination of heat pipes and heat sinks to capture and transfer heat effectively in a TEM has been proved successful even for ultra-low grade waste heat streams [35].

WHR concept using TEM are influenced by various types of heat sources where the modelling for the systems usually focuses on efficient and high-powered thermoelectric materials [36]. A steady-state model for engines was developed by He et al. [37] while Lan et al. [38] developed a model for dynamic thermal conditions. Also, Gu et al. [39] and Rejeb et al. [40] developed numerical models to explore the effectiveness of thermoelectricity for solar photovoltaic systems. Electrical power from wearables TEG by recovering heat from the human body is an advanced use of TEG cells. Moreover, models have been developed by Francioso et al. [41] and Soleimani et al. [42] to identify the optimal conditions for this specialized application. Borcuch et al. [43] developed a numerical model to specifically analyse TEG outputs for a hexagonal heat exchanger with different

fin designs where 350W of electrical power was reported. Bismuth telluride is the most common thermoelectric material [44] used with a maximum temperature of 250°C [45]. The operating temperature of TEG cells is dependent on the material type and to generate significant electricity, there must be a large temperature difference between the cell surfaces. One surface needs effective heating while the other surface requires active cooling to allow large quantities of heat to flow across the semiconductors. Theoretical modelling is needed to realize practical TEM designs for specific applications due to the unique geometrical and operating parameter constraints. The models would allow design optimization where parametric variations are a direct approach to analyse the sensitivity of the parameters to targeted outcomes and obtain a prediction of the performance.

There have been studies using the approach of varying TEM parameters to identify optimal conditions for thermoelectric power from industrial waste heat. A thermodynamic model by Meng et al. [46] simulated TEG cells in a gas-phase waste heat source. Variations on the fluid temperatures and heat transfer coefficients produced an optimal thermoelectric element length. It was concluded that the TEG power is most sensitive to the heat transfer coefficient, but a balanced performance can be obtained by controlling the cooling water temperature. An optimal 4.5% conversion efficiency was obtained for an element length of 2mm. A model by Børset et al. [47] based on a silicone casting furnace proved that TEM power outputs are highly influenced by the active cooling conditions. The sensitivity of TEM to cooling conditions has led to different proposals to enhance thermal dissipation. A system using a thermosyphon heat exchanger by Araiz et al. [48] improved the power generation up to 36%. Mirhosseini et al. [49] applied pin-fin heat sinks on their TEM design for a cement rotary kiln. Their model showed that staggered pin-fins performed better than an in-line arrangement with a maximum power output of 105.9 W/m2. Wang et al. [50] used high-temperature potassium heat pipes to recover heat from a 630°C industrial heat source using the effective thermal conductivity method in their model. Zhao et al. [51] concluded that the heat pipes addition in a TEG system increased the TEG conversion efficiency at high heating power due to lower thermal resistance along the heat pipes.

An integrated thermofluids and thermoelectric numerical model by Aranguren et al. [52] accounted for the Seebeck and Peltier effects and the temperature of the flue gas for a two-layer TEM exposed to high-temperature flue gas. Another model by Araiz et al. [53] proposed the use of fin dissipaters and thermosyphons on the TEG for cost optimization of heat recovery from a stone wool manufacturing plant. Variations to the ducting temperature, heat exchanger geometry and configurations, as well as power consumption by auxiliary equipment were conducted for performance optimization. Charilaou et al. [54] proposed a TEM for the cement industry where optimization for various design concepts proved the importance of the hot-side fin geometry in capturing the waste heat towards the overall TEM performance.

Different methods and techniques were used by researchers for TEM design optimization with one similar objective of obtaining the highest power output from the module. Parametric variation is among the acknowledged approach that provides a clear response of individual parameters on the generated electrical power. Bou et al. [19] applied a parametric variation approach to identify the best TEM configuration for minimum fuel consumption of an electric vehicle and Borcuch et al. [43] performed parameter sweep analysis on TEM hot side heat exchanger for optimum parallel-plate fin height and power output. Another parametrical analysis was conducted by He et al. [55] n solar heat pipe TEM, presenting the basic parameters influencing the power output and TEG conversion efficiency including the cooling water temperature and the number of thermoelements. Aliahmadi et al. [16] applied a genetic algorithm for multi-objective optimization for TEM integrated with three different ORC systems while Su et al. [56] combined genetic algorithm and response surface method for TEG heat exchanger in automotive application design optimization. A physics-based approach by Kishore et al. [57] was conducted for segmented TEG performance optimization. The combination of Analysis of variance (ANOVA) and Taguchi methods with the numerical simulation proved to reduce the number of experiments required by the conventional optimization methods. Abdelkareem et al. [58] gathered the advantages of nanofluids in increasing the heat transfer and pointed out the drawbacks for improvement in the future.

The TEM model considered in this study was based on a one-dimensional thermal resistance method by Remeli et al. [59]. Their validated model predicted the heat sink effectiveness, the heat transfer rate and the amount of power generated by a TEM involving energy recovery from an industrial waste heat stream at 75°C. The electrical power produced was predicted in a simplified approach by applying the rated efficiency of the TEG cells to the calculated heat transfer rate across the TEG cells. The rated cell efficiency was obtained experimentally, and it is a function of thermoelectric gradient [7]. The model was capable of predicting the exit temperature of the cold stream with less than a 3% difference to experimental results. However, the model did not feature the effects of heat exchanger orientations and the study was conducted for a low-temperature waste stream. Studies proved that heat flow through a TEM and its power generation is influenced by parameters such as temperature, thermal conductivity, electrical resistivity, current density and even distance between the hot and cold sides [60].

Remeli et al. [7] has firstly introduced the concept of heat pipe thermoelectric generator, followed by experimental and field studies by others. However, none of the studies

or current literatures incorporate the theoretical approach and parameter sweep analysis that would be more effective in the designing process of a TEM. Developing a WHR system involves complicated stages and without proper designing process, the design could be inefficient for waste heat capturing. Parameter sweep analysis is a continuous modelling that is needed to adapt the unique TEM WHR system features with the specific environmental conditions. Past reviews on theoretical modelling indicates that most researchers focused on design optimization by only varying specific working parameters without proper modelling of the individual parameters contributions. Parameter sweep method could be the conceptual guidance in improving TEM design and performance as the relative sensitivity of individual and crucial parameters could be obtained. This manuscript presents a novel evaluation by parameter sweep method on the responses of nine operating and geometrical parameters, under the possibility of four heat exchanger configurations of a TEM system developed for an industrial-scale CHP referring to the conditions of a baking factory. The method is based on a one-dimensional thermal resistance network and effectiveness-NTU model. The thorough evaluation and prediction method by using a steady-state and one-dimensional model aims to obtain faster and reliable results with shorter calculation time compared to three-dimensional computational modelling. As the TEM system includes a heat pipe analysis, the presented modelling is capable to prevent the complex numerical calculation involving multiphase without affecting the outcomes.

A TEM consisting of 2 TEG cells connected to two sets of heat pipe heat exchangers (HPHE) was designed to meet the dual function of electrical power generation and heating of a cold air stream. The validated model was applied to the TEM design to obtain its responses towards the heat transfer rate, electrical power generation and stream heating degree. This paper also highlights the various heat sink configurations for the TEM for performance investigation. Four novel TEM designs with different heat sink configurations are compared for a thorough analysis of the heat sink geometry.

The main objective of the analysis is to investigate the influence of each parameter on the TEM performance in meeting its CHP function. Another issue that was evaluated is the identification of the best configuration for the TEM relative to the HPHE orientation. Then, a new TEM design was proposed based on the information gained from the parametric analysis and its performance was compared with the initial design. The presented work contributes towards generating a better fundamental understanding of the TEM system characteristics at a level that can be applied for rapid design performance analysis of any new WHR designs to cater for the demand variations of specific industries.

SYSTEM DESCRIPTION

Waste Heat Recovery Domain

Figure 1 shows the domain for the WHR model based on a baking factory. The main baking oven releases waste heat and TEM recovers the waste heat and channels it to meet the heating demands of the proofing oven while generating electrical output. A higher heating degree of the cold air stream entering the proofing oven would translate into a reduction in power consumption needed for the electrical heaters at the proofing oven, as well as better waste heat energy utilization. Simultaneously, the TEG cells convert the waste heat into useful electrical power for local consumption of auxiliary devices such as the fan blowers for the ovens.

Thermoelectric Generator Module

The initial TEM design comprises two sets of heat pipe heat exchangers (HPHE) and two TEG cells sandwiched between two copper blocks as shown in Figure 2. Four heat pipes connect the copper block to each heat exchanger. The heat from the main oven, nominally at 250°C and 0.7 m/s [7], is captured by the hot-side HPHE and transferred to the copper block that houses the TEG cells. Power generation by the TEG cells is influenced by the rate of conduction heat transfer across the cells. This is assisted by the cold-side HPHE that transfers the heat to a low-temperature air stream (at a reference condition of 27°C and 0.7 m/s [7]) in a pre-heating process.

There are two initial HPHE designs (Design 1 and Design 2) that differ in the length of the heat sink as shown in Figure 2. $L_{HD,D1}$ has a length of 0.05m while $L_{HS,D2}$ is 0.15m. Both heat sinks have similar width (W_{HS}) and height (H_{HS}) of 0.15m and 0.16m. Using the two HPHE designs, four TEM configurations (labelled as C1 to C4) were developed

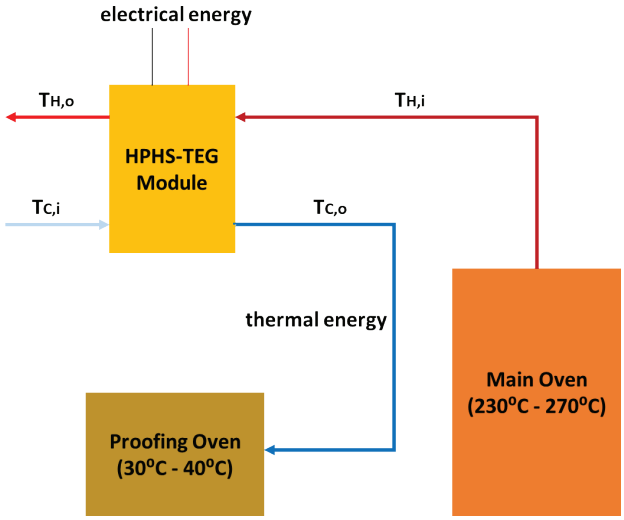

Figure 1. Process schematic of WHR from a baking factory.

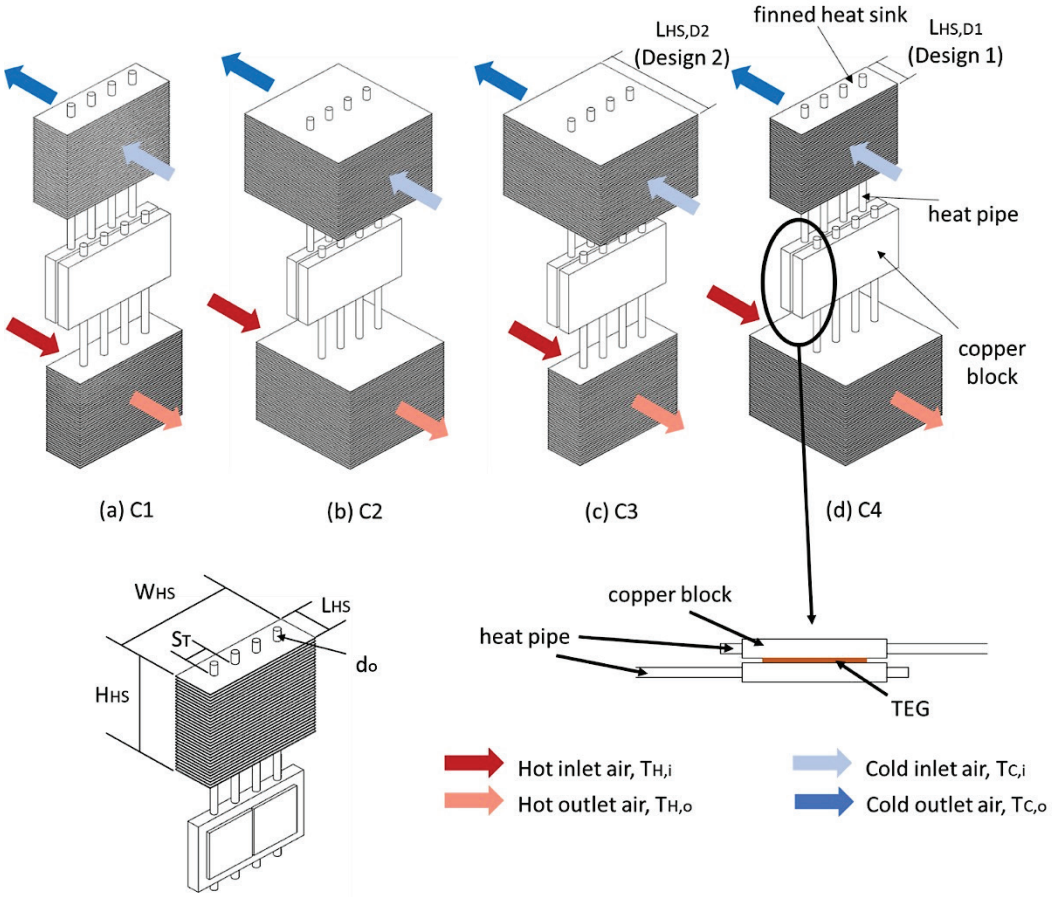

Figure 2. Base designs of HPHE (Design 1 and Design 2) with different fin lengths ($L_{HS,D1}$=0.05m and $L_{HS,D2}$=0.15m) applied to produce four TEM configurations.

for the parametric response analysis. Figure 2 displays the TEM configurations relative to the hot stream from the main oven and the cold stream to the proofing oven. Due to the required CHP functions, the TEM performance was evaluated based on both TEG power output and the regenerated heating effect of the cold stream. Therefore, varying the configurations would assist in obtaining an improved evaluation and understanding of the TEM characteristics. The detailed specifications of all the TEM components are provided in Table 1.

Thermal Resistance Network and NTU Effectiveness Method

The steady-state one-dimensional model was developed based on the thermal resistance network and NTU-effectiveness method. Forced convection mechanics is dominant at both HPHE as both fluid streams are induced using a momentum source (fans). The main outputs from the theoretical modelling are the power generated from the TEM (P_{TEM}) and the regenerated thermal energy.

Power generation

The power generated from the TEG cells, P_{TEM} is calculated by using the formula [61]

$$P_{TEM} = \mu_{TEM} Q_{TEM} \quad \text{(W)} \tag{1}$$

where μ_{TEM} is the TEG conversion efficiency and Q_{TEM} is the heat transfer rate across the TEG referred from Hosung et al. [61]. The μ_{TEM} is calculated with the formula

$$\mu_{TEM} = \left(1 - \frac{T_{C,TEG}}{T_{H,TEG}}\right)\left(\frac{\sqrt{ZT+1}-1}{\sqrt{ZT+1}+\frac{T_{C,TEG}}{T_{H,TEG}}}\right) \tag{2}$$

where $T_{C,TEG}$ and $T_{H,TEG}$ are the cold and hot-side surface temperatures of the TEG cell while ZT is the figure of merit of the TEG.

The figure of merit, ZT is calculated based on the formula [62]

$$ZT = \frac{S^2\sigma}{k}T \tag{3}$$

where S is the Seebeck coefficient, σ is the electrical resistivity and k is the thermal conductivity. The studies of

Table 1. Specifications of the TEM base designs

Parameter	Value	Unit
TEG cell		
L_{TEG}	0.062	m
W_{TEG}	0.062	m
t_{TEG}	0.00385	m
k_{TEG}	2.9799	W/m.K
HPHE		
$L_{HS,D1}$	0.05	m
$L_{HS,D2}$	0.15	m
W_{HS}	0.152	m
H_{HS}	0.16	m
N_{fin}	65	
t_{fin}	0.001	m
t_{gap}	0.002	m
k_{fin}	186	W/m.K
Heat pipe		
d_o	0.008	m
d_i	0.007184	m
d_v	0.007094	m
k_{hp}	401	W/m.K
N_w	600	
d_w	0.000045	m
Copper block		
t_{cb}	0.015	m
k_{cb}	385	W/m.K
A_{cb}	0.01672	m^2
Thermal paste		
t_{tp}	0.001	m
k_{tp}	14	W/m.K
A_{tp}	0.003844	m^2

thermoelectric material must effectively consider the effect of the temperature-dependence of the material. Table 2 shows an example of temperature-dependent polynomials of n-type and p-type thermoelectric material.

The outlet temperature of the cold air stream, $T_{C,o}$ is determined from the steady-flow energy balance of the cold stream [7], where

$$T_{C,o} = T_{C,i} + \frac{Q_{TEM}}{\dot{m}_C C_{p,C}} \ (°C) \tag{4}$$

where $\dot{m}_C$ is the mass flow rate of the cold air stream and $C_{p,C}$ is the specific heat of the cold air stream.

Under the steady-state assumption, the rate of heat transfer, Q_{TEM}, is based on the total thermal resistance, R_M across the TEM [61],

$$Q_{TEM} = \frac{\left(T_{H,i} - T_{C,i}\right)}{R_M} \ (W) \tag{5}$$

where $T_{H,i}$ and $T_{C,i}$ are the inlet temperatures of the hot air stream and cold air stream, respectively.

Thermal resistance network

Figure 3 shows the process diagram of the TEM with the equivalent thermal resistance network. There are nine thermal resistance elements involving convection at both HPHE and conduction across the heat pipes, copper block, thermal paste, and TEG cells. Specifications of each component in the TEM design applied in the analysis are listed in Table 1.

The parameter R_M is the total thermal resistance across the TEM. The thermal resistance of each component takes

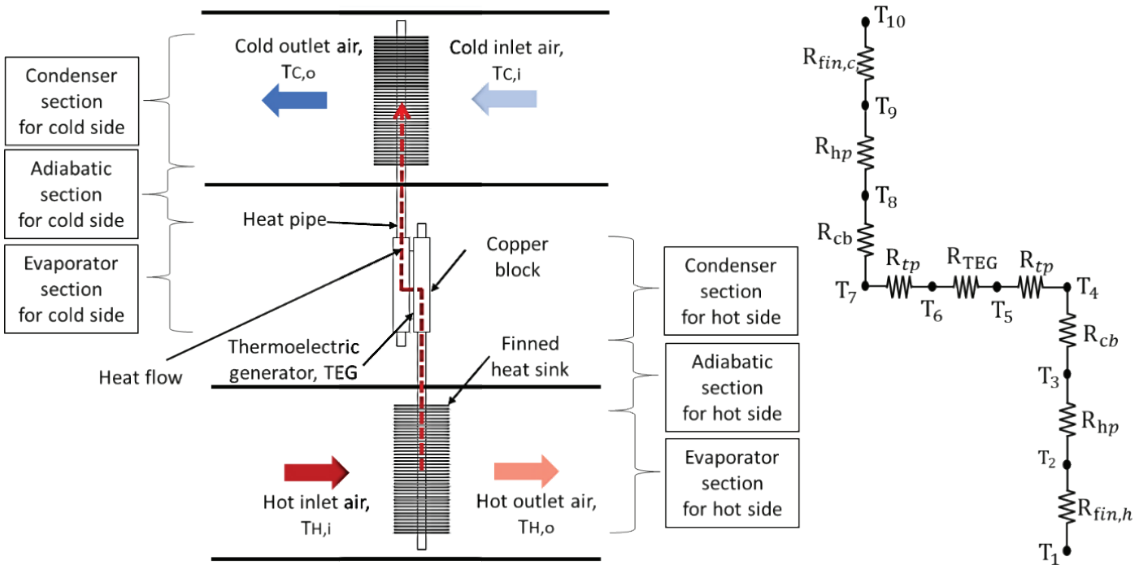

Figure 3. CHP process diagram of the TEM with the equivalent thermal resistance model.

Table 2. Temperature-Dependent Polynomials of Thermoelectric Materials Properties [63]

Properties	Polynomial Functions of Temperature	Temperature Range
	n-type	
S	$-10^{-6} \times [151.7414 + 0.226T + (1.574 \times 10^{-3}T^2) - (1.3005 \times 10^{-5}T^3) + (2.54021 \times 10^{-8}T^4) - (1.6143 \times 10^{-11}T^5)]$	$25 \leq T \leq 550$
σ	$10^{-5} \times [0.93562 + (4.321 \times 10^{-3}T) - (7.6044 \times 10^{-5}T^2) + (7.2921 \times 10^{-7}T^3) - (2.7176 \times 10^{-9}T^4) + (4.3202 \times 10^{-12}T^5) - (2.49 \times 10^{-15}T^6)]$	$25 \leq T \leq 550$
k	$1.2979 - (4.3139 \times 10^{-3}T) - (8.8823 \times 10^{-5}T^2) - (4.2988 \times 10^{-7}T^3)$	$25 \leq T \leq 100$
	$0.81325 + (1.0936 \times 10^{-2}T) - (7.454 \times 10^{-5}T^2) + (1.8004 \times 10^{-7}T^3) - (1.3833 \times 10^{-10}T^4)$	$100 \leq T \leq 400$
	$-4376.63 + 47.82405T - 0.2087T^2 + (4.548094 \times 10^{-3}T^3) - (4.950144 \times 10^{-7}T^4) + (2.15322 \times 10^{-10}T^5)$	$400 \leq T \leq 550$
	p-type	
S	$10^{-6} \times [208.4305 - 0.72663T + (2.3556 \times 10^{-2}T^2) - (3.265 \times 10^{-4}T^3) + (2.2189 \times 10^{-6}T^4) - (5.6125 \times 10^{-9}T^5)$	$20 \leq T \leq 170$
	$10^{-6} \times [512.3379 - 2.4027T + (4.8969 \times 10^{-3}T^2) - (4.13146 \times 10^{-6}T^3)]$	$170 \leq T \leq 450$
σ	$10^{-5} \times [1.14586 - (7.9785 \times 10^{-3}T) + (1.69084 \times 10^{-4}T^2) - (7.526 \times 10^{-7}T^3) + (1.33902 \times 10^{-9}T^4) - (8.9007 \times 10^{-13}T^5)]$	$20 \leq T \leq 450$
k	$0.874746 + (8.085 \times 10^{-3}T) - (3.63173 \times 10^{-5}T^2) - (1.16321 \times 10^{-6}T^3) + (1.345 \times 10^{-8}T^4) - (4.0425 \times 10^{-11}T^5)$	$20 \leq T \leq 170$
	$1.84097 - (4.511 \times 10^{-3}T) - (1.415 \times 10^{-5}T^2) + (7.033 \times 10^{-8}T^3)$	$170 \leq T \leq 370$
	$-234.94675 + 1.6305T - (3.69338 \times 10^{-3}T^2) + (2.74356 \times 10^{-6}T^3)$	$370 \leq T \leq 450$

into consideration the number of components and arrangements (series and parallel resistance). Equation 6 is the simplified total thermal resistance of the TEM which considered every connection of the components involved in the TEM.

$$R_M = \frac{R_{fin,h}}{4} + \frac{2R_{hp}}{4} + 2R_{cb} + \frac{2R_{tp}}{2} + \frac{R_{TEG}}{2} + \frac{R_{fin,c}}{4} \quad (^oC/W) \quad (6)$$

where, $R_{fin,h}$, R_{hp}, R_{cb}, R_{tp}, R_{TEG}, and $R_{fin,c}$ are the thermal resistances of heat exchanger fins at the hot air stream, heat pipes, copper blocks, thermal paste, TEG cells and heat exchanger fins at the cold air stream, respectively.

The thermal resistance at both heat exchangers ($R_{fin,h}$ and $R_{fin,c}$) are similar and is dictated by forced convection mechanics [7],

$$R_{fin} = \frac{1}{\mu_o h_{air} A_t} \quad (^oC/W) \quad (7)$$

where μ_o is the overall surface efficiency (as in Eq. 8) [7], h_{air} is the heat transfer coefficient (refer Eq. 11) and A is the total surface area.

$$\mu_o = 1 - \left(\frac{N_{fin} A_f}{A_t}\right)\left(1 - \mu_f\right) \quad (8)$$

where N_{fin} is the number of fins, A_f is the fin area while μ_f is the fin efficiency that can be obtained from [7,64].

$$\mu_f = \frac{\tanh mL_{HS}}{mL_{HS}} \quad (9)$$

The parameter L_{fin} is the fin length and m represent the relationship between the thermal conductivity and the heat transfer coefficient of [45].

$$m = \sqrt{\frac{2h_{air}}{k_{fin} t_{fin}}} \quad (10)$$

The parameters k_{fin} and t_{fin} are the thermal conductivity and thickness of the fin, respectively.

The h_{air} measures the effective heat transfer interaction between the fluid streams and the fin surfaces. The h_{air} at both heat exchangers is determined similarly based on Eqs. 11 [64].

$$h_{air} = \frac{Nu.k_{air}}{d_o} \quad (W/m^2.{}^oC) \quad (11)$$

where k_{air} is the thermal conductivity of air (either hot or cold streams, at film temperature) while d_o is the outer diameter of the heat pipe.

The Nusselt number, Nu, is a dimensionless number representing complex heat transfer interactions of convection mechanics. Based on Zukauskas [65]

$$Nu = 0.27\, Re^{0.63} Pr^{0.36} \left(\frac{Pr}{Pr_s}\right)^{0.25} \quad (12)$$

where Pr is the Prandlt number and the ratio Pr/Pr_s is considered as 1 at both HPHE due to the gaseous phase of both fluid streams.

The dimensionless Reynolds number [7],

$$\mathrm{Re} = \frac{\rho V_{\max} D_{hydraulic}}{\mu} \quad (13)$$

where ρ is the density of air, V_{max} is the maximum air velocity, $D_{hydraulic}$ is the hydraulic diameter and μ is the dynamic viscosity of the fluid. The $D_{hydraulic}$ is calculated from [66]

$$D_{hydraulic} = \frac{4 A_{free} L_{HS}}{A_e} \ \text{(m)} \quad (14)$$

where A_{free} is the free flow area (Eq. 15), A_e is the total heat transfer area (Eq. 16) and L_{HS} is the length of fins [66].

$$A_{free} = \left(\frac{S_T - d_o}{S_T}\right) L_e W_{HS} \ (\mathrm{m}^2) \quad (15)$$

$$A_e = \pi d_o L_e N_{HP} \ (\mathrm{m}^2) \quad (16)$$

The S_T is the transverse pitch, which is the distance between the heat pipes, while d_o is the outer diameter of the heat pipe, L_e is the heat pipe evaporator length, W_{HS} is the width of the heat sink, and N_{HP} is the number of the heat pipe.

The thermal resistance of a heat pipe, R_{hp}, is the combined resistances of the evaporator, the adiabatic and the condenser sections [7].

$$R_{hp} = R_{p,e} + R_{w,e} + R_{w,c} + R_{p,c} \ (^{o}\mathrm{C/W}) \quad (17)$$

The $R_{p,e}$ and $R_{w,e}$ are the radial and liquid wick combination resistance for the evaporator section of the heat pipe while $R_{p,c}$ and $R_{w,c}$ denotes the radial and liquid wick combination resistance for the condenser section, respectively.

The radial resistance, R_p [7],

$$R_p = \frac{\ln \frac{d_o}{d_i}}{2\pi L_{e,c} k_{HP}} \ (^{o}\mathrm{C/W}) \quad (18)$$

where d_o and d_i are the outer and inner diameter of the heat pipe while $L_{e,c}$ is the length of the evaporator or condenser sections, and k_{HP} refers to the thermal conductivity of the heat pipe.

The liquid wick combination resistance, R_w [7],

$$R_w = \frac{\ln \frac{d_i}{d_v}}{2\pi L_e k_{eff}} \ (^{o}\mathrm{C/W}) \quad (19)$$

where, d_v is the vapour spacing while k_{eff} is the effective thermal conductivity that can be calculated with[7]

$$k_{eff} = \varepsilon k_l + k_w (1 - \varepsilon) \ (\mathrm{W/m.^{o}C}) \quad (20)$$

The parameters k_l and k_w are the thermal conductivities of water and wick, respectively. The wick porosity, ε, is obtained from [7]

$$\varepsilon = 1 - \left(\frac{1}{4}\pi 1.05 N d_w\right) \quad (21)$$

where N is the number of copper mesh in the heat pipe and dw is the wire diameter of the mesh.

The copper block is a housing for the TEG cells. It consists of two plates with the TEG cells sandwiched between the plates. High conductivity thermal paste attaches the TEG cells to the copper block. From Fourier's law of conduction, the individual thermal resistances of these components can be calculated using the general expression [67],

$$R = \frac{t}{kA} \ (\mathrm{W/m.^{o}C}) \quad (22)$$

where t, k, and A are the individual thickness, thermal conductivity, and area, respectively, of the copper block, thermal paste, and TEG cells.

Model Validation

The validation of the TEM model was performece by comparing five theoeretical outputs with experiment results published by Zamri et al. [68]. The experimental setup from the lab-scale testing is shown in Figure *4*. Heat gun was used to imitate the hot air stream while DC fan functioned to accelerate the fluid stream with the required velocity. For the validation, the TEM design specifications and operating conditions are listed in Table 3, were similar to the design produced by the reference work.

As shown in Figure *5*(a) and Figure *5*(b) proved that the modelling predicted the temperature of fins on both hot and cold air streams with accuracy. The difference between theoretical and experiment is only 1% to 2%. The complexity of the TEG cell were successfully modelled as shown in Figure *5*(c) and Figure *5*(d), where the temperature of both TEG surfaces were predicted with error less than 10%. Lastly, Figure *5*(e) compared the electrical power output from the experiment with the value predicted by the proposed modelling. The percentage error varied between 2%

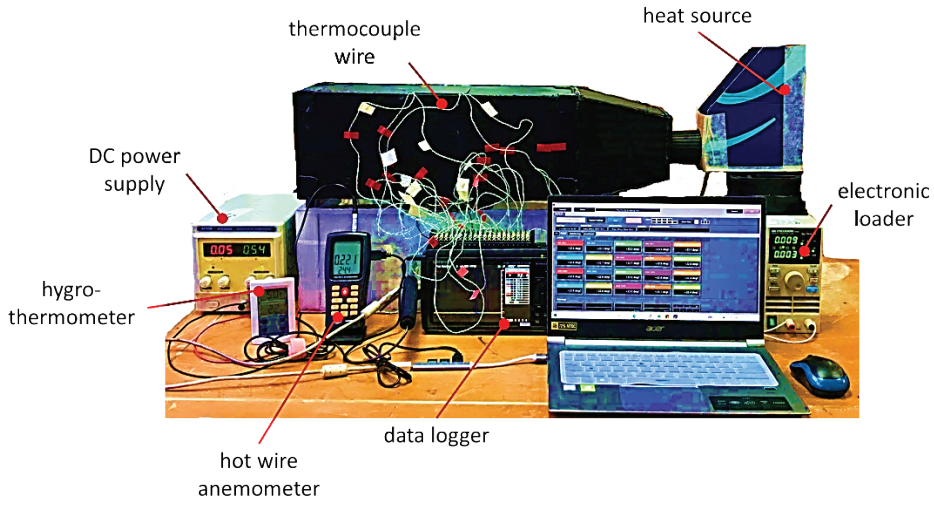

Figure 4. Experimental Setup [From Zamri et al. [68], with permission from JMechE.].

Table 3. TEM design and operating specifications used for model validation

Parameter	Value	Unit
TEG cell		
L_{TEG}	0.04	m
W_{TEG}	0.04	m
t_{TEG}	0.003	m
k_{TEG}	1.6	W/m.K
Operation		
$T_{H,i}$	80	°C
$T_{C,i}$	22	°C
$V_{H,i}$	0.7	m/s
$V_{C,i}$	0.7	m/s
Heat Sinks		
L_{HS}	0.045	m
W_{HS}	0.117	m
H_{HS}	0.109	m
N_{fin}	55	
t_{fin}	0.001	m
Heat pipe		
d_o	0.006	m
d_i	0.005184	m
d_v	0.005094	m
k_{hp}	401	W/m.K
N	600	
d_w	0.000045	m
Thermal paste		
t_{tp}	0.0005	m
k_{tp}	3	W/m.K
A_{tp}	0.0016	m^2

to 7%. However the mean difference is only 4% which is considered acceptable. From the comparison, the predicted output values using the one-dimensional model is satisfactory to be applied in the parametric variation analysis of the new TEM designs and configurations.

Parameter Sweep Approach

The main objective is to evaluate the end results of the design and operating parameters to the TEM performance. Varying the parameters individually while maintaining the interconnection and analysing its outputs is known as the parameter sweep approach. Nine parameters were chosen and the responses on heat transfer across the TEG module (Q_{TEM}), electrical power output (P_{TEM}), and outlet temperature of the cold air stream ($T_{C,o}$) were analysed. As in Figure 6, the chosen parameters were on the operation (temperature and velocity of fluid streams) and design (fin heat exchanger geometries, number of heat pipes and TEG cells). Along with the parametric variation analysis, four design configurations were compared and evaluated.

For the first parameter sweep, the effect of hot air stream temperature ($T_{H,i}$) from 100°C to 400°C at constant inlet hot air stream velocity ($V_{H,i}$) of 0.7 m/s was investigated. The reference temperature was 250°C (main oven exhaust temperature). The second analysis is on the effect of $V_{H,i}$ varied from 0.7 m/s to 2.4 m/s at a constant $T_{H,i}$ of 250°C with nominal $V_{H,i}$ of 0.7 m/s [7]. Table 4 lists the corresponding hot stream Reynolds number (Re_H) for the applied velocities of each TEM configuration. Varying the $V_{H,I}$ produce similar Re_H for C1 and C3 while C2 is similar to C4 due to the difference in hydraulic diameter of the configurations.

Next, the analysis focused on the geometrical parameters of both HPHE (as in Figure 2). The modelling was separated based on the hot and cold streams for each parameter.

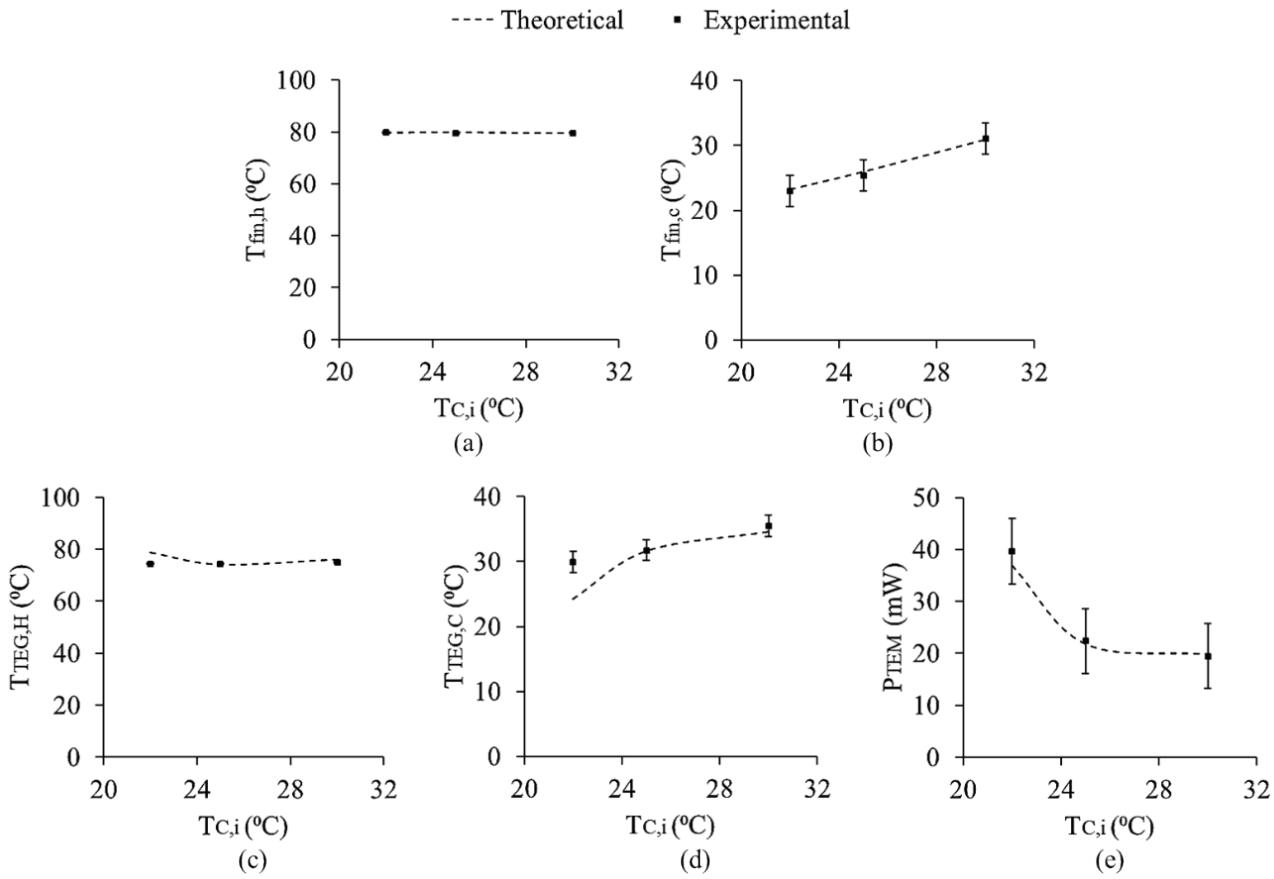

Figure 5. Theoretical outputs compared to experimental data [From Zamri et al. [68], with permission from JMechE.].

The third variation was on the heat sink length (L_{HS}). For Design 1 with a shorter length ($L_{HS,D1}$), the length was varied from 0.03m to 0.12m. For Design 2, the length ($L_{HS,D2}$) was varied from 0.102m to 0.327m. The fourth variation was on the heat sink width (W_{HS}) from 0.102m to 0.327m. The fifth variation was on the heat sink height (H_{HS}) from 0.16m to 0.51m.

The sixth parameter variation was on the number of heat pipes (N_{HP}) from 1 to 8 units. Initially, the distance between the heat pipes was 0.0304m and the maximum heat pipe that can be installed was 4 units. As more heat pipes were added (N_{HP}= 5-8), the distance reduces in an equal division. Then, the number of TEG (N_{TEG}) cells was varied from 2 to 8 with increments of 2 cells. The area of the copper blocks increased accordingly to the changes in N_{TEG}.

The final two-parameter sweeps focused on the inlet temperature ($T_{C,i}$) and velocity ($V_{C,i}$) of the cold stream. The $T_{C,i}$ was varied from 25°C to 35°C at a velocity of 0.7 m/s. The final parametric change varied the $V_{C,i}$ from 0.7

Table 4. Re_H and Re_C for the TEM configurations

Velocity	Re_H		Re_C	
	C1&C3	**C2&C4**	**C1&C4**	**C2&C3**
0.7	21582	65610	40392	15472
1.1	32373	98414	60589	23209
1.5	43164	131219	80785	30945
1.9	53955	164024	100981	38681
2.1	59351	180426	111079	42549
2.3	70142	213231		

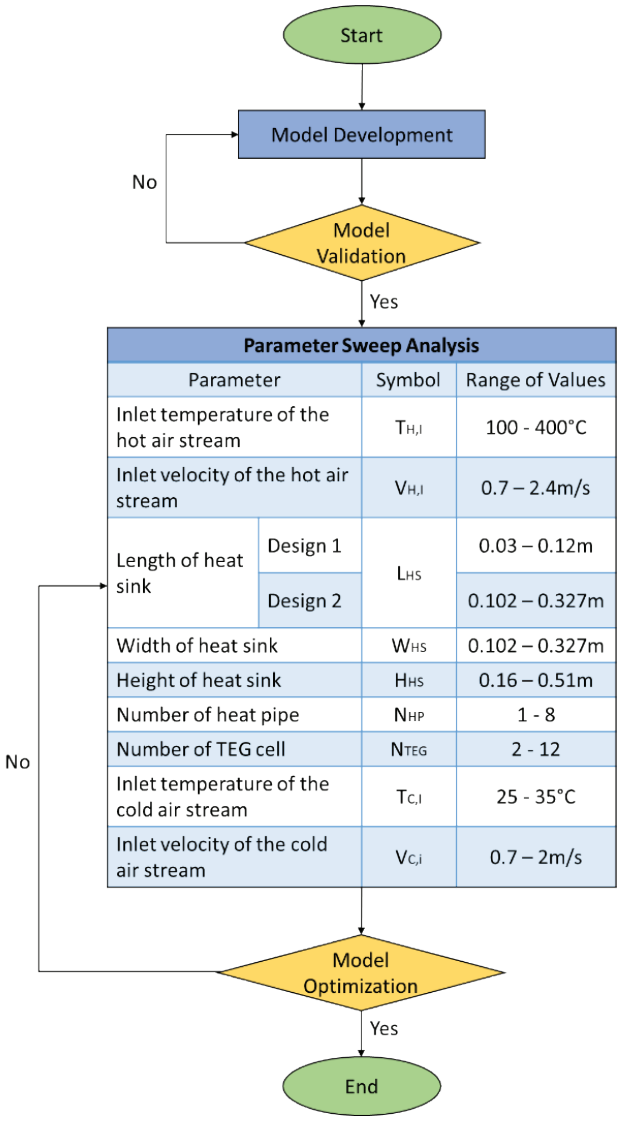

Figure 6. Flow of the parametric variation analysis with details of the parameters.

m/s to 2.1 m/s while the $T_{C,i}$ was constant at 30°C. The Reynolds number of the cold stream (Re_C) for each configuration is tabulated in Table 4. Configurations C1 and C4 have similar Re_C while C2 has similar values with C3.

PARAMETER SWEEP ANALYSIS

Hot Stream Parameters

Effects of inlet temperature, $T_{H,i}$

Figures 7(a) and 7(b) displayed a linear increase in Q_{TEM}, P_{TEM} and $T_{C,o}$. If the main oven produces hot gas at 100°C, the predicted Q_{TEM} was only 300W, but it has the potential to increase to 1600W if the $T_{H,i}$ increases to 400°C. The TEM designs allow an increase in Q_{TEM} at a rate of approximately 4.3 W/°C with slight variations for each configuration. Relatively, the P_{TEM} increased from 6W to 44W at a rate of 0.13 W/°C. The results are theoretically valid as a high hot stream temperature increases the thermal potential for heat transfer and create higher electron excitations within the TEG cells for electrical power generation. Configuration C2 registered the highest Q_{TEM} and P_{TEM}, followed by C3, then C4, and finally C1. Configuration C2 has the advantage of higher $D_{hydraulic}$ at both HPHE, leading to higher Re. As a consequence, higher convection rates were achieved and translated into higher Q_{TEM}. However, the change in $T_{H,i}$ from 100°C to 400°C at a constant velocity only produced a 4% difference in Q_{TEM} between C2 and C1, meaning it can be expected that there is only a small difference in performance between the TEM configurations. In Figure 7(c), the temperature increase for the cold air stream was linear with less than 4% difference across the configurations. At $T_{H,i}$=100°C, the predicted $T_{C,o}$ was 36°C and it increased to 48°C at $T_{H,i}$=250°C and 60°C at $T_{H,i}$=400°C. The linear relationships indicate that the TEM heated the cold air stream at approximately 8°C for every 100°C increase in $T_{H,i}$ when the stream velocity is constant at 0.7 m/s.

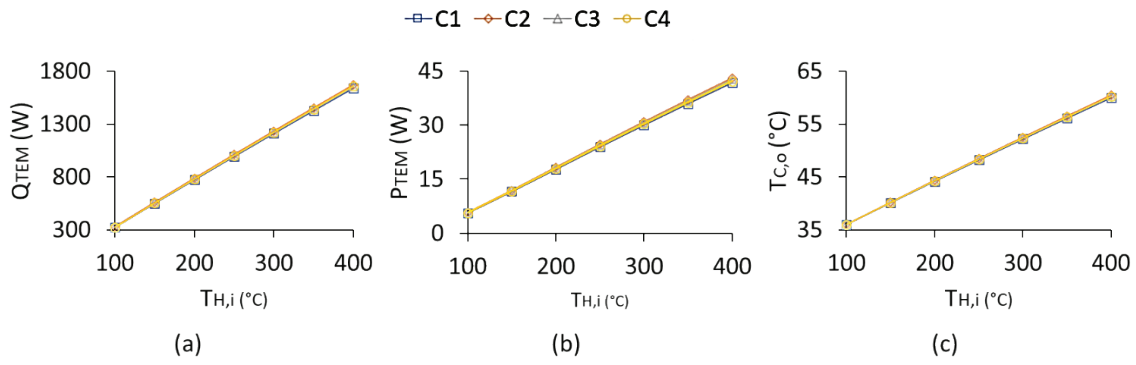

Figure 7. Effects of $T_{H,i}$ to the output parameters.

Effects of inlet velocity, $V_{H,i}$

The second parameter sweep varies the $V_{H,i}$ from 0.7 m/s to 2.4 m/s at a constant $T_{H,i}$=250°C. In Figure 8, each configuration showed a similar profile - a sharp increase as the velocity increases from 0.7 to 1.3 m/s followed by a significantly lower increase rate. Luo et al. [69] also observed that TEG output power was highly influenced by the waste heat temperature and mass flow rate where the power augments constantly with the increase in heat source velocity. In Figure 8(a), the initial increase in Q_{TEM} was 3 to 4% from the base heat transfer value. Then, the Q_{TEM} was constant between 1030 to 1045W, where configuration C2 gave the highest outputs. The maximum Q_{TEM} increase across all configurations was approximately 5%. The initial increase for P_{TEM} was in the range of 8 to 9%, then the increase was insignificant after $V_{H,i}$=1.3 m/s. Configuration C2 gave the best output at 26.9W while C1 was lowest at 26W (a 4% difference with C2). The power outputs when $T_{H,i}$=250°C, and $V_{H,i}$=0.7 m/s was 25W. Therefore, increasing the $V_{H,i}$ by double only improved the maximum P_{TEM} by a range of 4 to 8%.

Initially, the $T_{C,o}$ increase across all configurations were approximately 1.5% (between 48.4°C to 49.1°C) where configuration C2 gave the highest output due to its higher corresponding Q_{TEM}. When $V_{H,i}$ exceeded 1.3m/s, the change in heating degree was too small. The convection heat transfer at the fin surfaces is limited by the conduction heat transfer rates across the components. Even though the heat capacity increases as the $V_{H,i}$ increases, the thermal balance of the design has been reached leading to very low increases for Q_{TEM}, P_{TEM} and $T_{C,o}$ when the $V_{H,i}$ was greater than 1.3 m/s.

Heat Exchanger Geometry

Effects of heat sink length, LHS

The geometrical study on length variation is divided according to the hot (Figure 9(a)-9(c)) and cold sides (Figure 9(d)-9(f)) of the TEM. Therefore, the graphs are

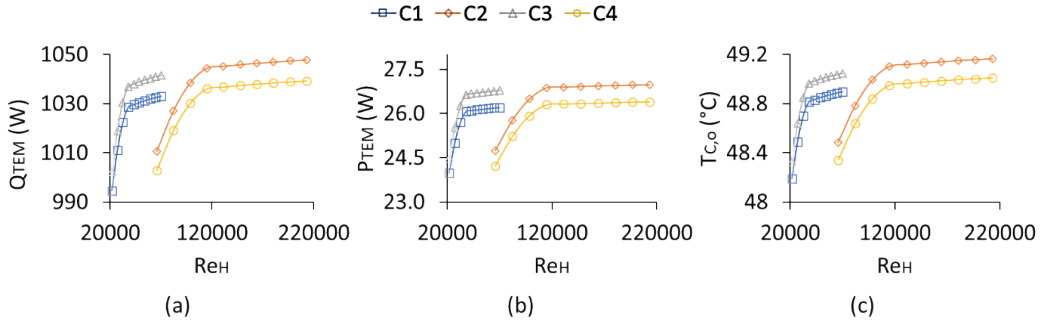

Figure 8. Effect of changes in $V_{H,i}$ (represented by Re_H).

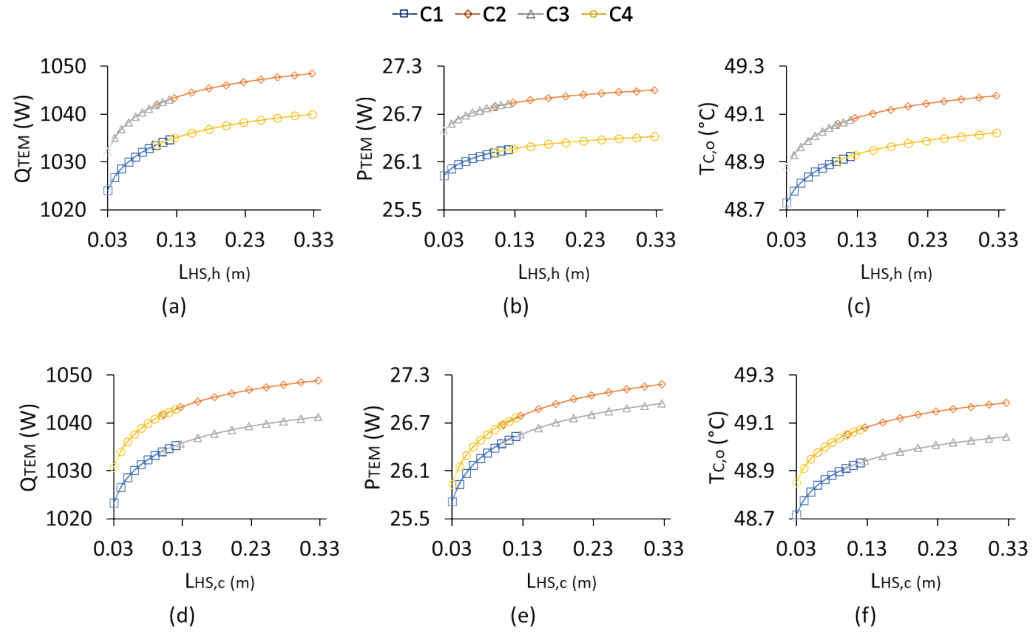

Figure 9. Effects of hot and cold-sides L_{HS} changes.

separated according to the relative L_{HS} values of each configuration. All output profiles show a non-linear increase as the L_{HS} was increased. On the hot side, a maximum 0.6% increase in Q_{TEM} from the initial design was obtained while the cold-side improvement was 0.7%. The P_{TEM} profile change was less than 0.1% while the $T_{C,o}$ increased by only 0.3% when the length changes at both hot and cold sides. Therefore, the extension of the L_{HS} at both ends of the module has no significant effect on all outputs.

Effects of heat sink width, WHS

Figure 10 shows that the increase of W_{HS} on both HPHE increased the Q_{TEM}, P_{TEM}, and $T_{C,o}$ in a non-linear profile where it approaches constant values due to geometrical constraints that limited the fin effectiveness. Tripling the W_{HS} at the hot-side HPHE from 0.102m to 0.327m enhanced the Q_{TEM} between 2 to 3% for all configurations, while the enhancement was 2 to 4% for the cold side. The W_{HS} affects the frontal area that receives the fluid streams and the convection surface area. A larger frontal area enhances the Re, while a larger fin surface area increases the fluid-surface interaction mechanics. The P_{TEM} increased by 0.7 to 1.2W for the hot-side width variation. However, the P_{TEM} increase was higher between 1.5 to 2W when the W_{HS} was varied at the cold side. This indicates that downstream conditions have a significant influence on the TEM outputs.

On the hot side, a W_{HS} of 0.127m for C1, C3, and C4 was sufficient for optimum power output. For configuration C2, maintaining the W_{HS} at the initial 0.15m was predicted to be sufficient. On the cold side, widening the heat sink to 0.177m for C1 and C4 led to an increase in power output to 26.2W and 26.6W, respectively. For C2 and C3, maintaining the initial W_{HS} was adequate as further increase merely led to a 1% increase in P_{TEM}. A total increase to the TC,o by 0.4 to 0.6°C, or 1% from its initial value, was predicted for all configurations.

Effects of heat sink height, HHS

In Figure 11, changes to the output parameters were minimal as the H_{HS} was varied from 0.16m to 0.51m at both sides of the TEM. The maximum Q_{TEM} increase was only 0.6%, between 0.5 to 0.7% for P_{TEM}, and the $T_{C,o}$ increment was only by 0.1°C. In this study, the changes to the heat exchanger height did not change the number of fins and its surface area. The fin gaps were doubled and this increases the frontal area for improved fluid flow into the heat exchangers, but the increase in Re was too small for significant changes to the outputs. Therefore, maintaining the initial H_{HS} for both sides of the TEM is predicted to be sufficient since the P_{TEM} increase was only 0.2W.

Module Specifications

Effects of number of heat pipes, NHP

Installation of additional heat pipes has a drastic effect only when the heat pipes were doubled from a single unit to two units where a 3 to 7% increase can be traced for the three outputs (refer to Figure 12). However, the increase is negligible as more heat pipes are added. The nominal design of 4 heat pipes was sufficient as installing more heat pipes contributed less than a 1% power increase. The parallel

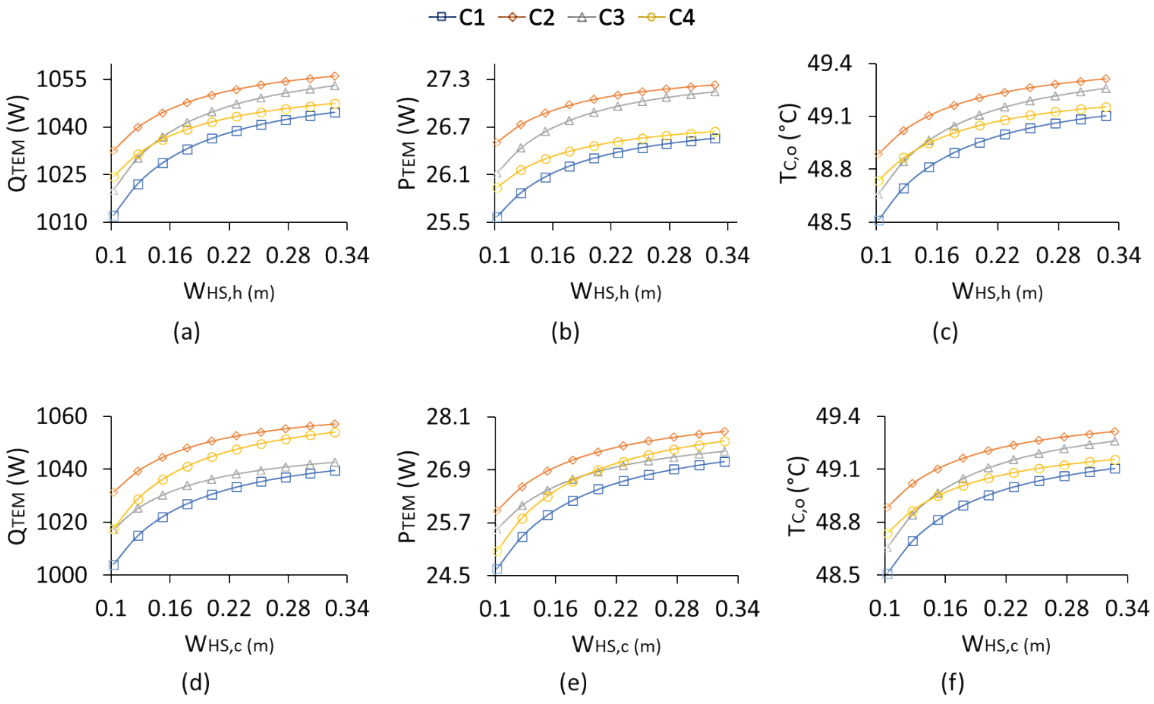

Figure 10. Effects of hot and cold-side W_{HS} changes.

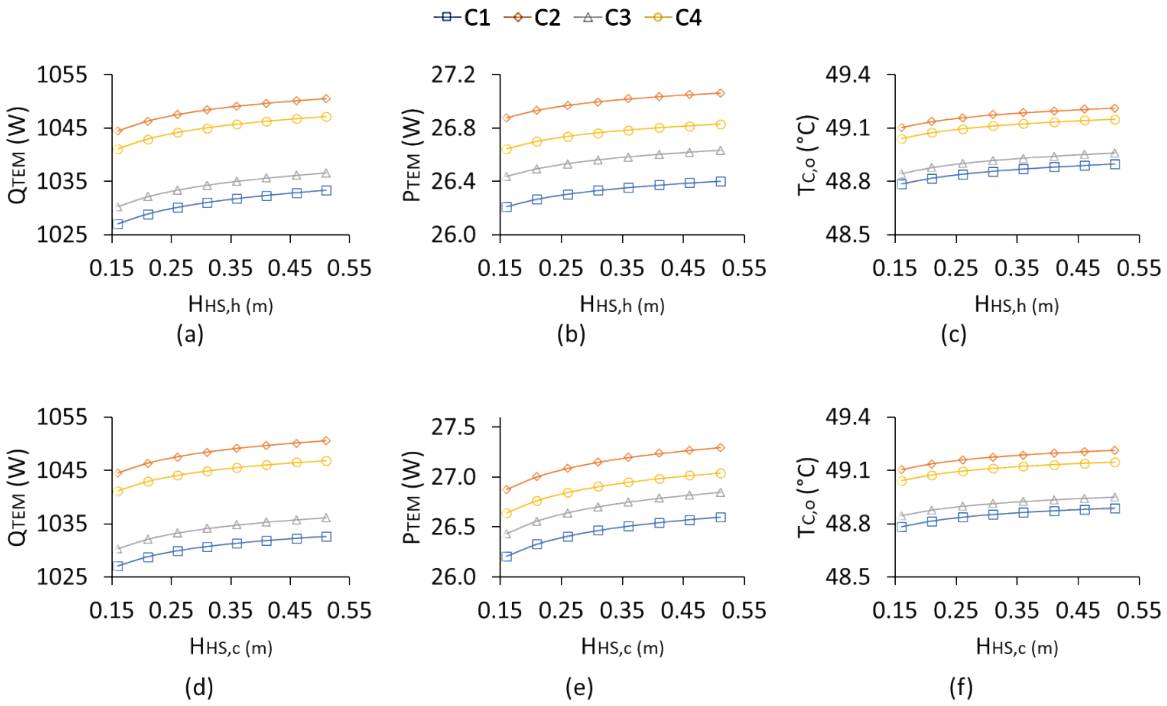

Figure 11. Effects of hot and cold side H_{HS} variations.

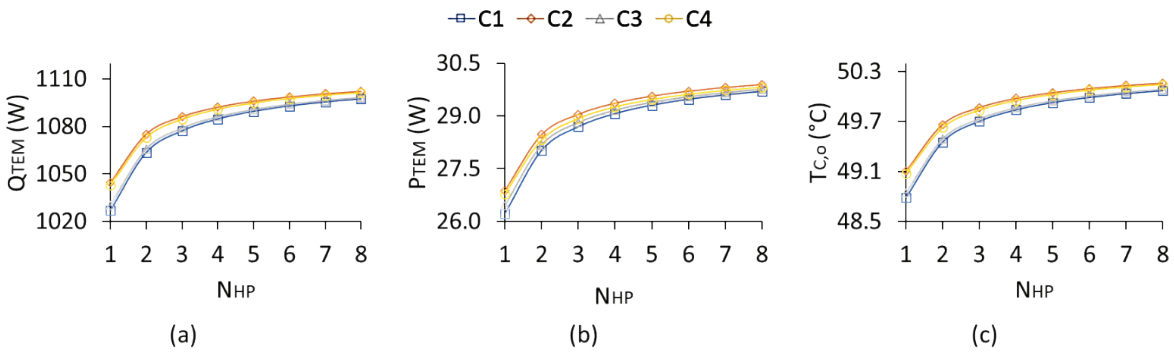

Figure 12. Effects of varying the N_{HP}.

contribution of the heat pipes in the thermal resistance limits the effect of heat pipe units on the heat flow magnitude. A comparison between 2 and 4 heat pipes indicates that the P_{TEM} increased by 12% across all configurations. Therefore, the N_{HP} factor is technically significant for a more positive techno-economic prospect for TEM designs.

The $T_{C,o}$ increase was small even when high N_{HP} were used. Compared to a single heat pipe, using 4 heat pipes only increased the outlet temperature by 3% and a further 2% for 8 heat pipes. Relatively, the temperature may reach 50°C using just 4 heat pipes for C2 and C4, while C1 and C3 needed 8 heat pipes to reach a similar temperature. It is expected that the real effect of increasing the N_{HP} can only be seen under a transient state where it improves the time to reach steady-state conditions at the TEG cells as well as for the cold stream preheating process.

Effects of TEG cell units, NTEG

Figure 13 showed the addition of N_{TEG} produced an increase in Q_{TEM}, a mixed profile for P_{TEM}, a reduction in ΔT_{TEM}, and an increasing trend for $T_{C,o}$. The increase in TEG cells leads to an increase in the heat transfer surface area and a subsequent decrease in the thermal resistance at the copper block. Therefore, the steady-state heat transfer rate significantly increases. However, the effect on power output is not as direct since it is dependent on the quality of ΔT_{TEM}. Referring to Equation 2, the reduction of the ΔT_{TEM} will reduce the maximum conversion efficiency (μ_{TEM}) and in turn, will reduce the power output.

In Figure 13(a), the intersection of the Q_{TEM} and the μ_{TEM} lines is the optimum point to the power output. At 6 TEC cells per module, configuration C2 produced the maximum P_{TEM} at 88W. Increasing the N_{TEG} by more than 6 units leads to a reduction in the electrical power. The addition of cells led to a decrease in ΔT_{TEM} (refer to Figure 13(c)). This resulted in a large reduction of μ_{TEM} from 0.028 at 2 cells to only 0.005 at 12 cells (as shown in Figure 13(a)). For heating of the cold air stream as in Figure 13(d), configuration C2 gave the best heating effect across all N_{TEG}, allowing the cold air to be heated to 210°C when 12 cells were used. Accounting for both functions of CHP, the TEM design with 6 TEG cells is the best choice due to the lower P_{TEM} registered at higher N_{TEG}.

Cold Stream Operating Conditions

Effects of inlet temperature, $T_{C,i}$

Based on the initial 2 TEG cell designs, the $T_{C,i}$ was increased from 25°C to 35°C. Figure 14(a) indicates a higher Q_{TEM} across the module when $T_{C,i}$ was lower. Configurations C2 and C4 showed a 3 to 4% higher heat transfer range (1060W to 1120W) than those produced by C1 and C3. At 25°C, the P_{TEM} was approximately 12% higher compared to at 35°C across all the configurations (Figure 14(b)). The result is similar to the findings of Alam et al. [15] where the TEG power output showed a visible increase when the cooling source temperature is reduced.

The uniform decrease in Q_{TEM} and P_{TEM} was due to the smaller temperature difference between the TEG cell

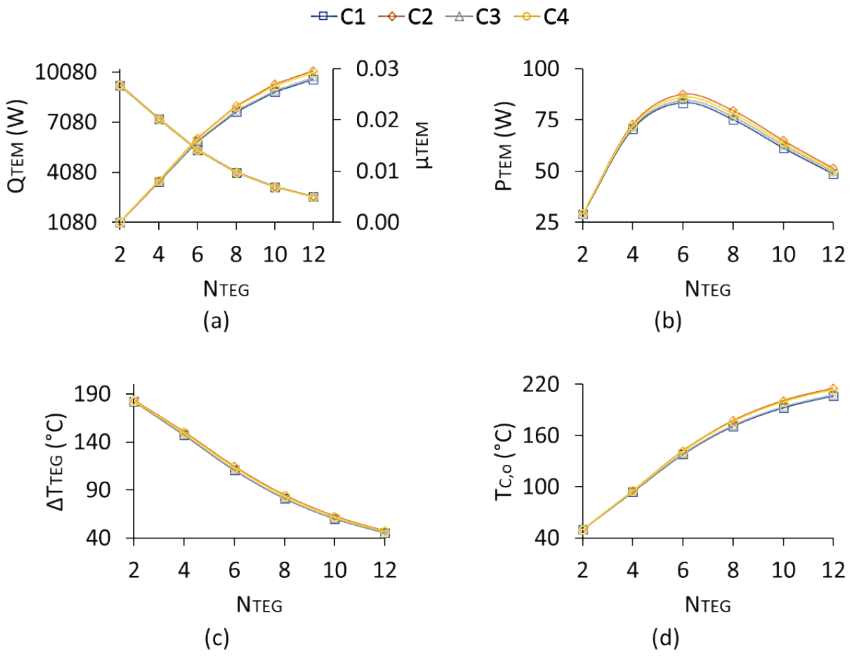

Figure 13. Effects of increasing the N_{TEG}.

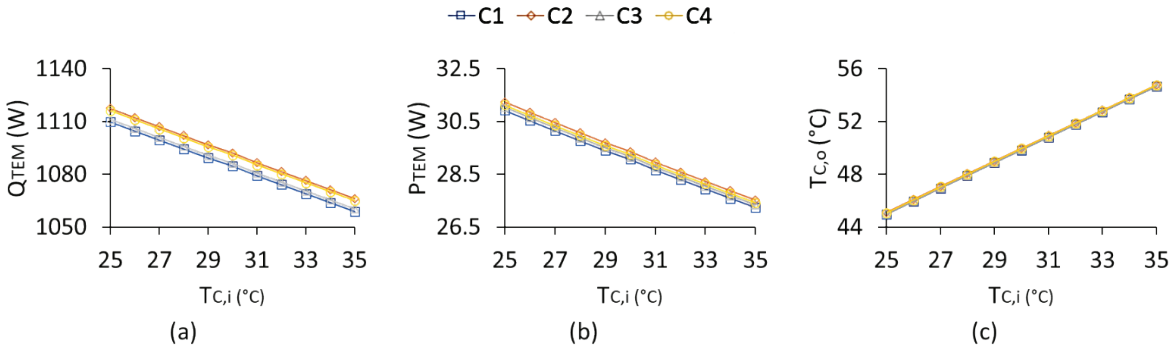

Figure 14. Effects of $T_{C,i}$ changes.

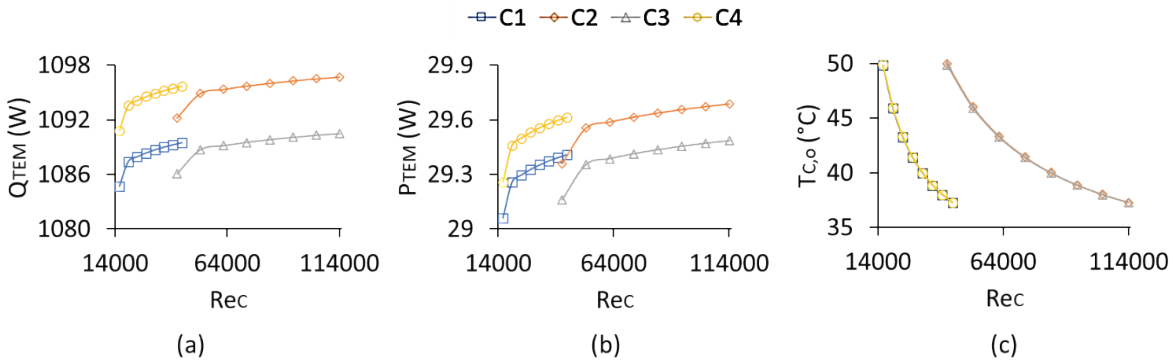

Figure 15. Effects of varying $V_{C,i}$.

surfaces and the air stream when the cold air inlet temperature increases. Therefore, it can be expected that the TEM design would generate a 12% higher power output during night operation ($T_{C,i}$= 25°C) compared to operation during a hot afternoon ($T_{C,i}$= 35°C). In Figure 14(c), a 5% linear increase in $T_{C,O}$ can be expected for all configurations even though the heat transfer reduces.

Effects of inlet velocity, $V_{C,i}$

The last parametric variation traces the effects when the $V_{C,i}$ was increased from 0.7 m/s to 2.1 m/s while the inlet temperature was constant at 30°C. The profiles for Q_{TEM} and P_{TEM} in Figure 15(a) and (b) were similar where a sharp enhancement was followed by a marginal increase as the Re_C increased. The effective total increase in Q_{TEM} was merely 4%. The cost-effectiveness of the fan power supply is an issue for cold air supply beyond this velocity, which was a critical point highlighted by Luo et al. [69] in their study to limit the parasitic losses of TEM designs.

Evidently, configurations C2 and C4 produced higher Q_{TEM} and P_{TEM} compared to C1 and C3. At the velocity of 2 m/s, the Q_{TEM} for C2 and C4 were in the range of 1096W to 1097W (approximately 3.5% higher than C1 and C3) while the corresponding P_{TEM} was between 29.6W to 29.7W (approximately 4.7% higher than C1 and C3). In contrast, Figure 15(c) predicted an exponential decline to the $T_{C,o}$ for all the configurations due to the inherent 'cooling effect' of larger air flow rates related to the thermal capacity and the rate of heating of the air stream. A 13°C temperature drop can be expected when the $V_{C,i}$ was increased from 0.7 m/s to 2.1 m/s due to the increase in heat capacity.

Overall Responses for Improved TEM Design

Table 5 tabulates the main responses for each case. Varying the geometrical aspects of the base designs have a low impact on the outputs compared to changes in other aspects. However, the fin width factor may lead to visible output improvements in the outputs and can be accounted for in the design if space limitation is not an issue. The optimal heat sink width is lower for the hot-side (0.127 - 0.15m) compared to the cold-side HPHE (0.15 to 0.177m). Due to the low temperatures of the cold stream, the heat sink effectiveness can be improved by providing a larger frontal area (influenced by the change in width), which in turn balances the potential heat flow from a higher temperature stream with smaller HPHE on the hot-side.

The outputs were more responsive to changes in the cold stream conditions than the hot stream, as was also observed by Børset et al. [47]. Under steady-state assumptions, the overall heat flow through the TEM was limited by the combined factors of heat capacity of the cold stream and the thermal resistance at the cold-side HPHE. Therefore, low cold stream temperatures at high Re_C produced significantly higher Q_{TEM} and leading to enhanced P_{TEM}. However, higher flow rates at the cold-side led to lower $T_{C,o}$ even if the Q_{TEM} was increased due to the chill effect of fluid streams with higher mass. Therefore, an optimal flow rate of the cold stream should be based on the targeted cold stream temperature needed for the proofing oven.

The number of heat pipes and TEG cells contributed significantly to the outputs. The optimal numbers were 4 heat pipes and 6 TEG cells. However, if the prime objective of the TEM is the cold stream heating effect, then higher numbers of TEG cells can be applied. It is important to note that the heating effect contributed a higher percentage to the overall energy recovery of the waste heat stream.

These results are comparable to the findings by Charilaou et al. [54] that fin width at the hot-side heat exchanger is a dominant factor in optimizing the power output of TEG cells. They also found no significant increase in TEG power due to cooling stream velocity. In contrast, they stated that the TEG cell number is the least influential which disagrees with the results of our work. However, their TEM was not designed for CHP and it does not incorporate heat pipes and heat exchange blocks to house the TEG cells that significantly lowered the thermal resistance within the whole module. Therefore, it can be concluded that unique TEM designs produce different parametric hierarchies relative to their performance.

Table 5. Summary of the parameter variation analysis on the TEM outputs

Parameter	*QTEM*	*PTEM*	$T_{C,O}$
Hot air stream			
1. $T_{H,i}$ (100 - 400°C)	4.3 W/°C	0.13 W/°C	8°C per 100°C
2. $V_{H,i}$ (0.7 - 2.4 m/s)	5% max increase	9% max increase	18 to 19°C heating degree
Heat sink geometry			
1. L_{HS}			
i. Hot-side (tripled)	0.6% increase (4 – 8W)	< 0.1% increase	0.3% increase (0.2°C)
ii. Cold-side (tripled)	0.7% increase (5 -12W)	< 0.1% increase	0.3% increase (0.1°C)
2. W_{HS}			
i. Hot-side (tripled)	2-3% increase (18 – 28W)	3 – 5% increase (0.7 – 1.2W)	1% max increase (0.4-0.6°C)
ii. Cold-side (tripled)	3-4% increase (20 – 30W)	7 – 8% increase (1.5 - 2W)	1% max increase (0.4-0.6°C)
3. H_{HS}			
i. Hot-side (tripled)	0.6% max increase (4W)	0.5 – 0.7% increase (0.2W)	0.1°C increase (0.1°C)
ii. Cold-side (tripled)	0.6% max increase (4W)	0.6 – 0.7% increase (0.3W)	0.2% increase (0.1°C)
Module specifications			
1. N_{HP} (1 to 8 units)	5 - 7% increase (55 – 60W)	8 - 12% increase (3 – 3.5W)	3% max increase (0.4°C)
2. N_{TEG} (2 to 12 cells)	10x increase	3x max. increase Max. 6 cells	5x increase
Cold air stream			
1. $T_{C,i}$ (25 – 35°C)	3-4% decrease (60W)	12% decrease (3.7W)	5% increase (9°C)
2. $V_{C,i}$ (0.7 – 2 m/s)	4% max increase	3.5 – 4.7% increase	25% decrease

Energy Recovery Ratio Analysis

An improved TEM design (labelled as Design 3) was conceptualized from the optimal values of each parameter. The main differences are on the N_{TEG} where 6 TEG cells were applied, and the hot-side heat sink width was reduced to 0.127m. Other parameters were similar to the base design values of Design 2 with 2 TEG cells. An analysis was performed to compare the energy recovery ratio at the reference temperatures and velocities ($T_{H,i}$=250°C; $V_{H,i}$=0.7 m/s; $T_{C,i}$=30°C; $V_{C,i}$=0.7 m/s) for both fluids.

The energy recovery ratio, ε_R, was calculated based on

$$\varepsilon_R = \frac{P_R}{P_{H,i}} \quad (\%) \tag{a}$$

where the recovered thermal power, P_R is the total energy recovered via the TEG cells (P_{TEM}) and the heating of the cold stream (P_C),

$$P_R = P_{TEM} + P_C \quad (\mathrm{W}) \tag{b}$$

$$P_C = \dot{m}_C C_{p,C}\left(T_{C,O} - T_{C,i}\right) \quad (\mathrm{W}) \tag{c}$$

The available thermal power in the hot stream, $P_{H,i}$ is determined using

$$P_{H,i} = \dot{m}_H C_{p,H}\left(T_{H,i} - T_\infty\right) \quad (\mathrm{W}) \tag{d}$$

where T_∞ = 30°C (surrounding temperature) due to thermodynamic limitations.

Table 6. Output comparisons between the TEM base Design 2 and new Design 3

Parameter		Initial Design for C2 Design 2	New Design Design 3
Available thermal power in the hot stream	$P_{H,i}$ (W)	7231.64	6817.80
Cold outlet air temperature	$T_{C,o}$ (°C)	48.49	76.98
Heating rate of the cold stream	P_C (W)	1010.70	2568.92
Electrical power from TEG cells	P_{TEM} (W)	24.73	48.94
Total Recovered thermal power	P_R (W)	1035.43	2617.87
WHR ratio	ε_R (%)	14%	38%

Table 6 lists the comparative results between Design 2 and Design 3 for the C2 configuration. The N_{TEG} was multiplied by 3 (2 to 6 cells), but the generated P_{TEM} was magnified by 2 due to the series-parallel arrangement of the cells within the housing that limits the total power output. The increase factor for $T_{C,o}$ was 1.6. The enhanced outputs for P_{TEM} and $T_{C,o}$ were expected due to the higher heat transfer rate across the TEM for Design3 as the use of 6 TEG cells provided a larger surface area for heat transfer across the copper block housing. It is concluded that the outputs are directly proportionate to the increase of the copper block surface area.

The most significant outcome from the new Design 3 design is the enhanced ε_R. Design 2 only produced ε_R=14%, but it was enhanced by 2.7 times to ε_R=38% for Design 3. The proportions of energy transfer were almost similar for both designs - 98% of the recovered heat was transferred to the cold air stream heating and only 2% was converted into electrical power. Nevertheless, the modelling analysis has proved the potential of the proposed TEM design to reuse the waste heat from the main bakery oven for CHP application.

CONCLUSION

Waste heat recovery from the exhaust stream of the main oven in a bakery factory was studied using a specifically designed TEM. A one-dimensional heat transfer model was validated with the purpose to identify the specific characteristics and limitations of the designs. The parametric variation approach on the design and operating parameters of the TEM successfully identified the individual responses towards the Q_{TEM}, P_{TEM} and $T_{C,o}$. The parameter with the highest direct influence to enhance the outputs is the hot stream temperature. However, the cold stream conditions directly limit the effective heat transfer through the TEM. Profiles of the other parameters indicate that an effective performance enhancement is attainable only for a specific range. The parametric sweep approach on the design geometry indicates that the frontal area exposed to incoming fluid streams should be maximized, where the variation of fin width has a better effect than fin height at a similar number of fins. The heating degree of the cold air stream to be channelled into the proof oven is influenced by the convection heat transfer effectiveness at the cold-side HPHE. It is very sensitive to the $T_{C,i}$, which is a parameter linked to ambient conditions. Increasing the width of the cold-side HPHE also gives a significant improvement to the fin effectiveness and heating degree. Therefore, the cold-side HPHE should be designed larger than the hot-side HPHE.

The effect of hot-side and cold-side HPHE configurations was also studied. The four configurations displayed a good response towards the varied parameters due to adequate frontal area. Configuration C2 proved to be the best option to obtain an optimal CHP performance. The effective capture and release of thermal energy at both heat sinks are the key to enhanced TEM performance. The analysis also showed that the performance was significantly enhanced by increasing the surface area of the copper block that houses the TEG cells.

The WHR ratio indicates that a single TEM could only harvest a maximum of 14% of the total thermal power available in the waste heat stream from the main oven. It can be further increased using several modules in the series arrangement that can be the focus of future research. Also, by comparing the initial 2-cell design with a modified 6-cell design, the WHR ratio of a single module was enhanced significantly to 38% caused mainly by the increase in the copper block surface area.

Overall, the successful identification of the principal parameters would lead to greater comprehension of the intricate relationships of each design and operating component in the WHR domain. Comparing the parameter sweep approach to other recent 1-dimensional analysis, the method introduced in this manuscript is a new and unique technique to predict the outcome and to acquire the main parameter affecting the TEM system. The simplified calculations that avoid internal consideration of heat pipes and TEG cell have benefit this method compare to other approaches. The presented model and evaluation of results would assist in the development of practical and innovative designs by researchers and engineers to meet the WHR demands of various industrial applications towards contributing to the holistic agenda of sustainability.

NOMENCLATURES

ΔT_{PP}	pinch point temperature (°C)
ΔT_{TEM}	surface temperature difference of the TEG cells (°C)
A_{cb}	copper block surface area (m^2)
A_{TEG}	TEG cell surface area (m^2)
A_{tp}	thermal paste surface area (m^2)
d_i	inner diameter (m)
d_o	outer diameter (m)
d_v	vapour spacing (m)
d_w	wire diameter (m)
$H_{HS,c}$	height of cold stream heat sink (m)
$H_{HS,h}$	height of hot stream heat sink (m)
k_{cb}	copper block thermal conductivity (W/m.K)
k_{fin}	fin thermal conductivity (W.m/K)
k_{hp}	heat pipe thermal conductivity (W.m/K)
k_{TEG}	TEG cell thermal conductivity (W/m.K)
k_{tp}	thermal paste conductivity (W/m.K)
$L_{HS,c}$	length of cold stream heat sink (m)
$L_{HS,h}$	length of hot stream heat sink (m)
N_{fin}	number of fins
N_{HP}	number of heat pipes
N_{TEG}	number of TEG cells
N_w	number of wires
P_C	heating rate of the cold stream (W)
$P_{H,i}$	available thermal power in the hot stream (W)
P_R	recovered thermal power (W)
P_{TEM}	generated TEM electrical power (W)
Q_{TEM}	heat transfer rate across the TEM (W)
T_∞	surrounding temperature (°C)
$T_{C,i}$	cold stream inlet temperature (°C)
$T_{C,O}$	cold stream outlet temperature (°C)
$T_{C,TEG}$	TEG cold surface temperature (°C)
$T_{H,i}$	hot stream inlet temperature (°C)
$T_{H,O}$	hot stream outlet temperature (°C)
$T_{H,TEG}$	TEG hot surface temperature (°C)
t_{cb}	copper block thickness (m)
t_{fin}	fin thickness (m)
t_{gap}	fin gaps (m)
t_{TEG}	TEG cell thickness (m)
t_{tp}	thermal paste thickness (m)
$V_{C,i}$	cold stream inlet velocity (m/s)
$V_{H,i}$	hot stream inlet velocity (m/s)
$W_{HS,c}$	width of cold stream heat sink (m)
$W_{HS,h}$	width of hot stream heat sink (m)
ε_{HS}	heat sink effectiveness (%)
ε_R	waste heat recovery ratio (%)
μ_{TEM}	TEG conversion efficiency (%)

Abbreviations

CHP	combined heat and power
HPHE	heat pipe heat exchanger
HP-TEG	heat pipe thermoelectric generator
NTU	number of transfer units
Nu	Nusselt number
ORC	Organic Rankine Cycle
ReC	Reynolds number of the cold stream
ReH	Reynolds number of the hot stream
TEG	thermoelectric generator
TEM	thermoelectric module
WHR	waste heat recovery
ZT	figure of merit

ACKNOWLEDGEMENT

The authors would like to thank Universiti Teknologi MARA (UiTM) for the facilities and the Ministry of Higher Education Malaysia for the financial support given under research grants 600-RMC/KKP 5/3 (002/2021) and 600-IRMI/PRGS 5/3 (008/2019).

AUTHORSHIP CONTRIBUTIONS

Authors equally contributed to this work.

DATA AVAILABILITY STATEMENT

The authors confirm that the data that supports the findings of this study are available within the article. Raw data that support the finding of this study are available from the corresponding author, upon reasonable request.

CONFLICT OF INTEREST

The author declared no potential conflicts of interest with respect to the research, authorship, and/or publication of this article.

ETHICS

There are no ethical issues with the publication of this manuscript.

REFERENCES

[1] Huang F, Zheng J, Baleynaud JM, Lu J. Heat recovery potentials and technologies in industrial zones. J Energy Institute 2017;90:951−961. [CrossRef]

[2] Tchanche BF, Lambrinos G, Frangoudakis A, Papadakis G. Low-grade heat conversion into power using organic Rankine cycles - A review of various applications. Renew Sustain Energy Rev 2011;15:3963−3979. [CrossRef]

[3] Hamid Elsheikh M, Shnawah DA, Sabri MFM, Said SBM, Haji Hassan M, Ali Bashir MB, et al. A review on thermoelectric renewable energy: Principle parameters that affect their performance. Renew Sustain Energy Rev 2014;30:337−355. [CrossRef]

[4] Çelik FG, Açikkalp E, Yamik H. Performance assessment of phosphoric acid fuel cell - Thermoelectric generator hybrid system with economic aspect. J Therm Engineer 2018;5:29−45. [CrossRef]

[5] Ismail BI, Ahmed WH. Thermoelectric power generation using waste-heat energy as an alternative green technology. Recent Patents Electric Engineer 2009;2:27−39. [CrossRef]
[6] El-Adl AS, Mousa MG, Abdel-Hadi EA, Hegazi AA. Dynamic performance characteristics of a thermoelectric generator. J Therm Engineer 2019;5:385−395. [CrossRef]
[7] Remeli MF, Tan L, Date A, Singh B, Akbarzadeh A. Simultaneous power generation and heat recovery using a heat pipe assisted thermoelectric generator system. Energy Conver Manage 2015;91:110−119. [CrossRef]
[8] Fleurial JP. Thermoelectric power generation materials: Technology and application opportunities. J Mineral Metal Mater Soc 2009;61:79−85. [CrossRef]
[9] Venkatasubramanian R, Siivola E, Colpitts T, O'Quinn B. Thin-film thermoelectric devices with high room-temperature figures of merit. Nature 2001;413:597−602. [CrossRef]
[10] Chaturvedi E, Mamtani V. An investigative methodology through solid modelling and numerical analysis for designing a thermo-electric generator system. J Therm Engineer 2020;6:99−113. [CrossRef]
[11] Maneewan S, Chindaruksa S. Thermoelectric power generation system using waste heat from biomass drying. J Electron Mater 2009;38:974−980. [CrossRef]
[12] Kaibe H, Kajihara T, Fujimoto S. Recovery of plant waste heat by a thermoelectric generating system. Komatsu Tech Rep 2011;57:26−30.
[13] Meng F, Chen L, Sun F, Yang B. Thermoelectric power generation driven by blast furnace slag flushing water. Energy 2014;66:965−972. [CrossRef]
[14] Orr B, Singh B, Tan L, Akbarzadeh A. Electricity generation from an exhaust heat recovery system utilising thermoelectric cells and heat pipes. Appl Therm Eng 2014;73:588−597. [CrossRef]
[15] Alam M, Kumar K, Dutta V. Dynamic modeling and experimental analysis of waste heat recovery from the proton exchange membrane fuel cell using thermoelectric generator. Therm Sci Engineer Prog 2020;19:100627. [CrossRef]
[16] Aliahmadi M, Moosavi A, Sadrhosseini H. Multi-objective optimization of regenerative ORC system integrated with thermoelectric generators for low-temperature waste heat recovery. Energy Reports 2021;7:300−313. [CrossRef]
[17] Mohamed ES. Development and performance analysis of a TEG system using exhaust recovery for a light diesel vehicle with assessment of fuel economy and emissions. Appl Therm Eng 2019;147:661−674. [CrossRef]
[18] Liu C, Pan X, Zheng X, Yan Y, Li W. An experimental study of a novel prototype for two-stage thermoelectric generator from vehicle exhaust. J Energy Institute 2016;89:271−281. [CrossRef]
[19] Bou Nader W. Thermoelectric generator optimization for hybrid electric vehicles. Appl Therm Eng 2020;167:114761. [CrossRef]
[20] Chen J, Xie W, Dai M, Shen G, Li G, Tang Y. Experiments on waste heat thermoelectric generation for passenger vehicles. Micromachines (Basel) 2022;13:1−14. [CrossRef]
[21] Alegria P, Catalan L, Araiz M, Rodriguez A, Astrain D. Experimental development of a novel thermoelectric generator without moving parts to harness shallow hot dry rock fields. Appl Therm Eng 2022;200:117619. [CrossRef]
[22] Weng Z, Liu F, Zhu W, Li Y, Xie C, Deng J, et al. Performance improvement of variable-angle annular thermoelectric generators considering different boundary conditions. Appl Energy 2022;306:118005. [CrossRef]
[23] Chen J, Wang R, Luo D, Zhou W. Performance optimization of a segmented converging thermoelectric generator for waste heat recovery. Appl Therm Eng 2022;202:117843. [CrossRef]
[24] Alahmer A, Khalid MB, Beithou N, Borowski G, Alsaqoor S, Alhendi H. An experimental investigation into improving the performance of thermoelectric generators. J Ecological Engineer 2022;23:100−108. [CrossRef]
[25] Zheng LJ, Kang HW. A passive evaporative cooling heat sink method for enhancing low-grade waste heat recovery capacity of thermoelectric generators. Energy Conver Manage 2022;251:114931. [CrossRef]
[26] Badr F, Radwan A, Ahmed M, Hamed AM. An experimental study of the concentrator photovoltaic/thermoelectric generator performance using different passive cooling methods. Renew Energy 2022;185:1078−1094. [CrossRef]
[27] Mahdi MS, Abdulateef J, Abdulateef AM. Thermoelectric combined heat and power generation system integrated with Liquid-fuel stove. J Adv Res Fluid Mech Therm Sci 2018;51:19−30.
[28] Montecucco A, Siviter J, Knox AR. Combined heat and power system for stoves with thermoelectric generators. Appl Energy 2017;185:1336−1342. [CrossRef]
[29] Zhang Y, Wang X, Cleary M, Schoensee L, Kempf N, Richardson J. High-performance nanostructured thermoelectric generators for micro combined heat and power systems. Appl Therm Eng 2016;96:83−87. [CrossRef]
[30] Zarifi S, Mirhosseini Moghaddam M. Utilizing finned tube economizer for extending the thermal power rate of TEG CHP system. Energy 2020;202. [CrossRef]
[31] Zou WJ, Shen KY, Jung S, Kim YB. Application of thermoelectric devices in performance optimization of a domestic PEMFC-based CHP system. Energy 2021;229:120698. [CrossRef]

[32] Liu J, Shin KY, Kim SC. Comparison and parametric analysis of thermoelectric generator system for industrial waste heat recovery with three types of heat sinks: Numerical study. Energies (Basel) 2022;15. [CrossRef]
[33] Baroutaji A, Arjunan A, Ramadan M, Robinson J, Alaswad A, Abdelkareem MA, et al. Advancements and prospects of thermal management and waste heat recovery of PEMFC. Int J Thermofluids 2021;9:100064. [CrossRef]
[34] Cooper SJG, Hammond GP, Norman JB. Potential for use of heat rejected from industry in district heating networks, Gb perspective. J Energy Institute 2016;89:57−69. [CrossRef]
[35] Sulaiman MS, Singh B, Mohamed WANW. Experimental and theoretical study of thermoelectric generator waste heat recovery model for an ultra-low temperature PEM fuel cell powered vehicle. Energy 2019;179:628−646. [CrossRef]
[36] Zhang Y. Thermoelectric advances to capture waste heat in automobiles. ACS Energy Letters 2018;3:1523−1524. [CrossRef]
[37] He W, Wang S, Yue L. High net power output analysis with changes in exhaust temperature in a thermoelectric generator system. Appl Energy 2017;196:259−267. [CrossRef]
[38] Lan S, Yang Z, Chen R, Stobart R. A dynamic model for thermoelectric generator applied to vehicle waste heat recovery. Appl Energy 2018;210:327−338. [CrossRef]
[39] Gu W, Ma T, Song A, Li M, Shen L. Mathematical modelling and performance evaluation of a hybrid photovoltaic-thermoelectric system. Energy Conver Manage 2019;198:111800. [CrossRef]
[40] Rejeb O, Shittu S, Ghenai C, Li G, Zhao X, Bettayeb M. Optimization and performance analysis of a solar concentrated photovoltaic-thermoelectric (CPV-TE) hybrid system. Renew Energy 2020;152:1342−1353. [CrossRef]
[41] Francioso L, De Pascali C, Sglavo V, Grazioli A, Masieri M, Siciliano P. Modelling, fabrication and experimental testing of an heat sink free wearable thermoelectric generator. Energy Conver Manag 2017;145:204−213. [CrossRef]
[42] Soleimani Z, Zoras S, Ceranic B, Shahzad S, Cui Y. Optimization of a wearable thermoelectric generator encapsulated in Polydimethylsiloxane (PDMS): A numerical modelling. 2019 IEEE 2nd International Conference on Renewable Energy and Power Engineering, REPE 2019:212−215. [CrossRef]
[43] Borcuch M, Musiał M, Gumuła S, Sztekler K, Wojciechowski K. Analysis of the fins geometry of a hot-side heat exchanger on the performance parameters of a thermoelectric generation system. Appl Therm Eng 2017;127:1355−1363. [CrossRef]
[44] Angeline AA, Jayakumar J, Asirvatham LG, Wongwises S. Power generation from combusted 'Syngas' using hybrid thermoelectric generator and forecasting the performance with ANN technique. J Therm Engineer 2018;4:2149−2168. [CrossRef]
[45] Lan S, Yang Z, Chen R, Stobart R. A dynamic model for thermoelectric generator applied to vehicle waste heat recovery. Appl Energy 2018;210:327−338. [CrossRef]
[46] Meng F, Chen L, Feng Y, Xiong B. Thermoelectric generator for industrial gas phase waste heat recovery. Energy 2017;135:83−90. [CrossRef]
[47] Børset MT, Wilhelmsen Ø, Kjelstrup S, Burheim OS. Exploring the potential for waste heat recovery during metal casting with thermoelectric generators: On-site experiments and mathematical modeling. Energy 2017;118:865−875. [CrossRef]
[48] Araiz M, Martínez A, Astrain D, Aranguren P. Experimental and computational study on thermoelectric generators using thermosyphons with phase change as heat exchangers. Energy Convers Manag 2017;137:155−164. [CrossRef]
[49] Mirhosseini M, Rezania A, Rosendahl L. Power optimization and economic evaluation of thermoelectric waste heat recovery system around a rotary cement kiln. J Clean Prod 2019;232:1321−1334. [CrossRef]
[50] Wang C, Tang S, Liu X, Su GH, Tian W, Qiu S. Experimental study on heat pipe thermoelectric generator for industrial high temperature waste heat recovery. Appl Therm Eng 2020;175. [CrossRef]
[51] Zhao Y, Fan Y, Li W, Li Y, Ge M, Xie L. Experimental investigation of heat pipe thermoelectric generator. Energy Conver Manage 2022;252:115123. [CrossRef]
[52] Aranguren P, Araiz M, Astrain D, Martínez A. Thermoelectric generators for waste heat harvesting: A computational and experimental approach. Energy Conver Manage 2017;148:680−691. [CrossRef]
[53] Araiz M, Casi Á, Catalán L, Martínez Á, Astrain D. Prospects of waste-heat recovery from a real industry using thermoelectric generators : Economic and power output analysis. Energy Conver Manage 2020;205:112376. [CrossRef]
[54] Charilaou K, Kyratsi T, Louca LS. Design of an air-cooled thermoelectric generator system through modelling and simulations, for use in cement industries. Mater Today Proc 2019;44:3516−3524. [CrossRef]
[55] He W, Su Y, Riffat SB, Hou JX, Ji J. Parametrical analysis of the design and performance of a solar heat pipe thermoelectric generator unit. Appl Energy 2011;88:5083−5089. [CrossRef]
[56] Su CQ, Wang WS, Liu X, Deng YD. Simulation and experimental study on thermal optimization of the heat exchanger for automotive exhaust-based thermoelectric generators. Case Stud Therm Engineer 2014;4:85−91. [CrossRef]

[57] Kishore RA, Sanghadasa M, Priya S. Optimization of segmented thermoelectric generator using Taguchi and ANOVA techniques. Sci Rep 2017;7. [CrossRef]
[58] Abdelkareem MA, Mahmoud MS, Elsaid K, Sayed ET, Wilberforce T, Al-Murisi M, et al. Prospects of thermoelectric generators with nanofluid. Therm Sci Engineer Prog 2022;29:101207. [CrossRef]
[59] Remeli MF, Singh B, Affandi NDN, Ding LC, Date A, Akbarzadeh A. Investigation of counter-flow in a heat pipe-thermoelectric generator (HPTEG). J Electron Mater 2017;46:3115−3123. [CrossRef]
[60] Chandra V, Balasinorwala T, Dhokey NB. Dimensionless model and performance analysis of low temperature thermoelectric materials. Mater Today Proc 2021;43:3095−3099. [CrossRef]
[61] Lee HS. Thermal Design: Heat Sinks, Thermoelectrics, Heat Pipes, Compact Heat Exchangers and Solar Cells. New York: Wiley; 2010.
[62] Sempels EV, Kempers R, Lesage FJ. Load-bearing figure-of-merit characterization of a thermoelectric module. IEEE Trans Compon Packaging Manuf Technol 2016;6:50−57. [CrossRef]
[63] Barry M, Li J. Thermoelectric Performance of Novel Composite and Integrated Devices Applied to Waste Heat Recovery. J Heat Transf 2019;135.
[64] Huang GY, Hsu CT, Fang CJ, Yao DJ. Optimization of a waste heat recovery system with thermoelectric generators by three-dimensional thermal resistance analysis. Energy Conver Manage 2016;126:581−594. [CrossRef]
[65] Žukauskas A, Ulinskas R. Efficiency parameters for heat transfer in tube banks. Heat Transf Engineer 1985;6:19−25. [CrossRef]
[66] Kumar V, Gangacharyulu D, Tathgir RG. Thermal performance evaluation of heat pipe heat exchangers under natural convection. Int J Heat Exchangers 2006;7:103−122.
[67] Sulaiman MS, Singh B, Mohamed WANW. Experimental and theoretical study of thermoelectric generator waste heat recovery model for an ultra-low temperature PEM fuel cell powered vehicle. Energy 2019;179:628−646. [CrossRef]
[68] Zamri NF, Hamdan MH, Anuar SNA, Mohamed WANW, Remeli MF. Performance of a plate-finned thermoelectric generator (TEG) module for industrial waste heat recovery. J Mech Engineer 2022;19:257−272. [CrossRef]
[69] Luo D, Wang R, Yu W, Sun Z, Meng X. Theoretical analysis of energy recovery potential for different types of conventional vehicles with a thermoelectric generator. Energy Procedia 2019;158:142−147. [CrossRef]